Electronic Supplementary Information

Towards high-volumetric performance of Na/Li-ion batteries: A better anode material with molybdenum pentachloride–graphite intercalation compounds ($MoCl_5$-GICs)

Zheng Li,[a,b] *Chengzhi Zhang,* [a,b] *Fei Han,*[*a,b] *Fei Wang,*[a,b] *Fuquan Zhang,*[a,b] *Wei Shen,*[c] *Chong Ye,*[a,b] *Xuanke Li,*[a,b] *and Jinshui Liu*[*a,b]

[a] College of Materials Science and Engineering, Hunan University, Changsha 410082, China

[b] Hunan Province Key Laboratory for Advanced Carbon Materials and Applied Technology, Hunan University, Changsha, Hunan, 410082, China

[c] School of Environmental and Chemical Engineering, Jiangsu University of Science and Technology, Zhenjiang 212003, China.

Hunan University, Changsha, 410082, China

E-mail: feihan@hnu.edu.cn, Jsliu@hnu.edu.cn

Experimental section

Synthesis of $MoCl_5$-intercalated GICs: The $MoCl_5$-intercalated GICs were directly prepared by a molten-salt method. In a typical procedure, the raw materials of natural flake graphite (325 mesh, 99.95%, purchased from Laixi Graphite Trading Corp.), $MoCl_5$ and MoO_3 (purchased from Alfa Aesar) were firstly dried in a vacuum oven at 80 °C to remove the surface-adsorbed water. Then, 2.0 g of natural graphite flakes were quickly mixed with 10 g of $MoCl_5$ and 5g of MoO_3 salts in a mortar, and the mixture was placed into a sealed stainless-steel autoclave (Anhui Kemi Machinery Technology Co., Ltd). Subsequently, the autoclave was continuously heated at 350 °C for 24 h with a heating rate of 5 °C min^{-1}. After cooling, the powder was washed in turn with ethanol, 0.1M of HCl solution and deionized water to remove the residual reactants. After drying at 80 °C, the $MoCl_5$-intercalated GICs with stage 1 structure were obtained. The stage 2 $MoCl_5$-GICs were synthesized in the same procedure, except the mass of $MoCl_5$ was changed to 8 g and without the addition of MoO_3 salt.

Materials Characterizations: The crystal phase structure was monitored by X-ray powder diffraction on a TD-3300 diffractometer with Cu Ka radiation (λ = 1.5406 Å) at a scanning step of 0.02°. Raman spectrometry was operated by a Labram-010 system with an excitation laser of 514 nm in a spectral resolution of 1 cm^{-1}. The powder electronic conductivity was tested by a four-point probe method in an ST-2722 semiconductor resistivity powder tester. Scanning electron microscopy (SEM) and transmission electron microscopy (TEM) were carried out on Sigma HD and FEI-Tecnai/Titan G2 60-300 microscopes, respectively. X-ray photoelectron spectroscopy (XPS) was conducted on an ESCALAB 250XI spectrometer with a monochromatic Al Kα source. The data were calibrated with the C 1s binding energy of 284.6 eV.

Electrochemical Measurements: The electrochemical performance was tested by assembling CR2016/CR2025-type coin cells in an argon protected glovebox. The working electrodes were composed of 80 wt% active material, 10 wt% conducting agent of super P, and 10 wt% carboxymethyl cellulose binder on a Cu foil current collector. The typical mass loading of each disk was about 1.5 mg cm^{-2}. The lithium plate and sodium plate were used as the counter/reference electrodes for LIBs and SIBs, respectively. The electrolyte was a 1.0 M of $LiPF_6$ salt in ethylene carbonate (EC)/diethyl carbonate (DEC) (1:1 by volume) for LIBs, and 1.0 M of $NaPF_6$ in diglyme solution for SIBs without any additive. The galvanostatic discharge/charge tests were carried out on a Land CT2001A battery tester in a voltage range of 0.005–3 V. The cyclic voltammogram curves were recorded on a CHI660E electrochemical workstation in a potential window of 0.005–3.0 V. A Gamry interface 1000E electrochemical workstation was used to test the electrochemical impedance spectroscopy (EIS) from 100 kHz to 10 MHz frequency.

Computational methods: All calculations of binding energy and activation energy were performed using density functional theory (DFT) in the CASTEP program with the projector-augmented wave (PAW) method. The generalized gradient approximation (GGA) with Perdew-BurkeErnzerhof (PBE) functionals were used to describe exchange-correlation interaction of electrons with a cutoff energy of 520 eV. The threshold of convergence was set to be 1×10^{-5} eV and k-points sampling are generated automatically with 0.05 $Å^{-1}$ for structure relaxation. For instance, to model appropriate supercells for the $MoCl_5$/graphite layer structures, a supercell consisted of a 2×1×2 layer of $MoCl_5$ (010) and a 5×5×1 layer of graphite with lattice constants a = b = 12.99995 Å and c = 26.792214 Å was built. Similarly, a supercell consisted of a 4×4×1 layer of Mo (001) and a 3×3×1 layer of NaCl (100) with lattice constants a = b

= 11.92182 Å and c = 24.87631 Å was constructed. For all of the monolayer structural models, a vacuum layer of 15 Å was employed to avoid the interactions between the adjacent cells. The geometric structures were totally relaxed with a force convergence criterion of 0.01 eV $Å^{-1}$.

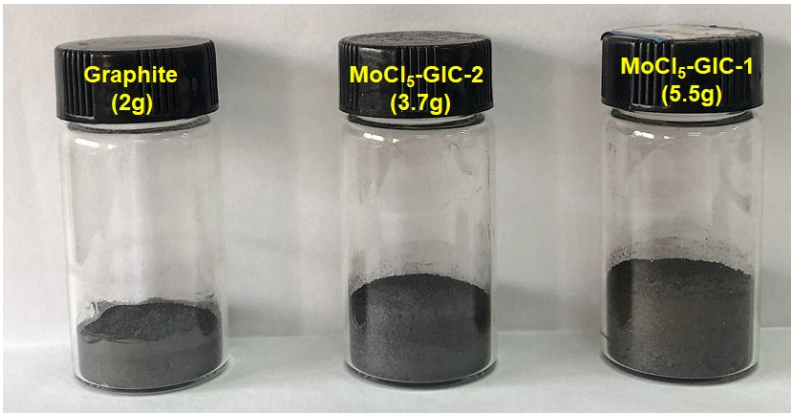

Fig. S1 The optical photo of pristine graphite and $MoCl_5$-intercalated GIC samples.

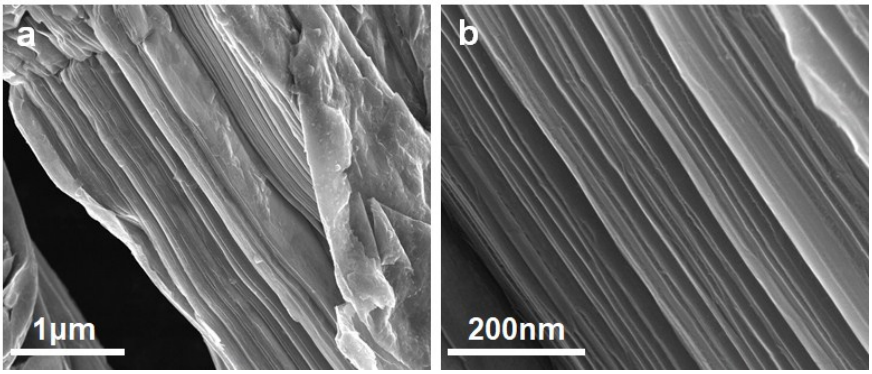

Fig. S2 SEM images of $FeCl_3$-GIC with stage 1 structure.

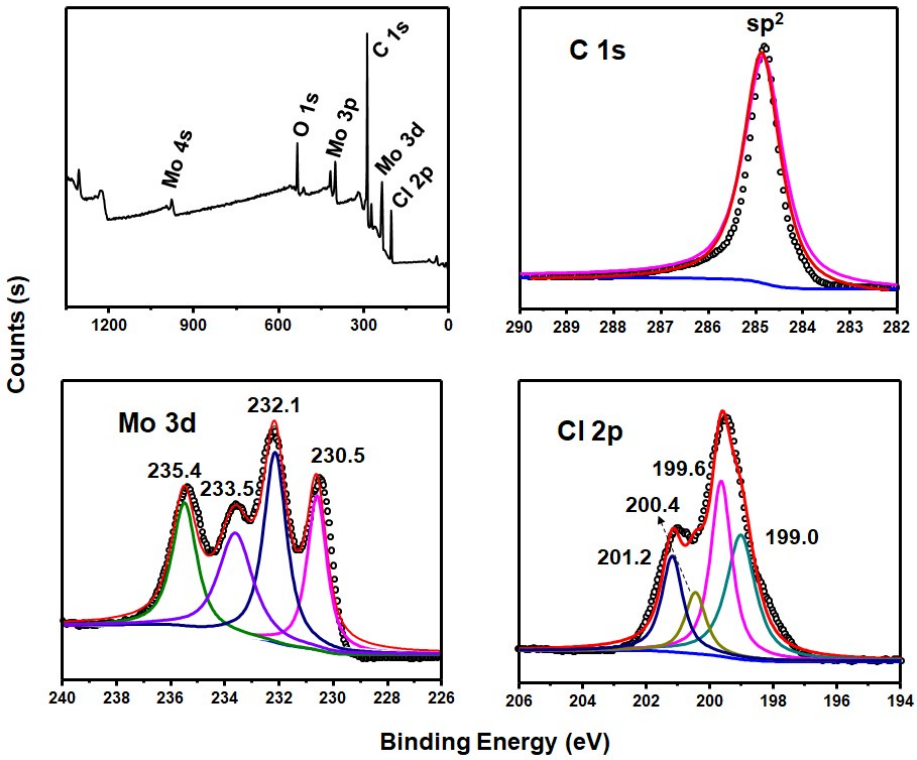

Fig. S3 XPS profiles of (a) $MoCl_5$-GIC-1, and its high-resolution spectra of (b) C 1s, (c) Mo 3d and (d) Cl 2p.

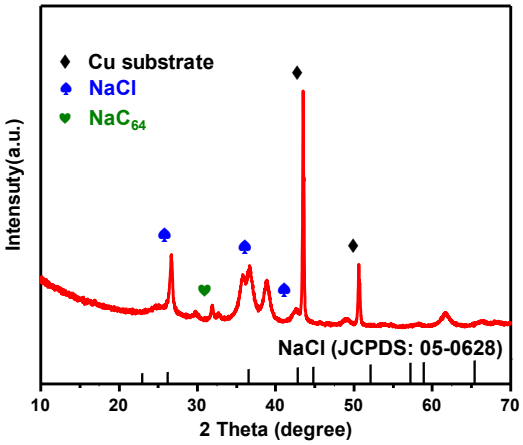

Fig. S4 XRD pattern of the $MoCl_5$-GIC-1 electrode at discharge to 0.96 V (vs. Na/Na^+).

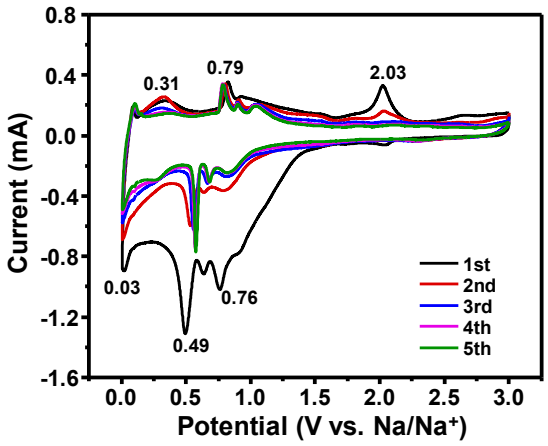

Fig. S5 Cyclic voltammograms of the $MoCl_5$-GIC-2 anode at 0.2 mV s^{-1} for SIBs.

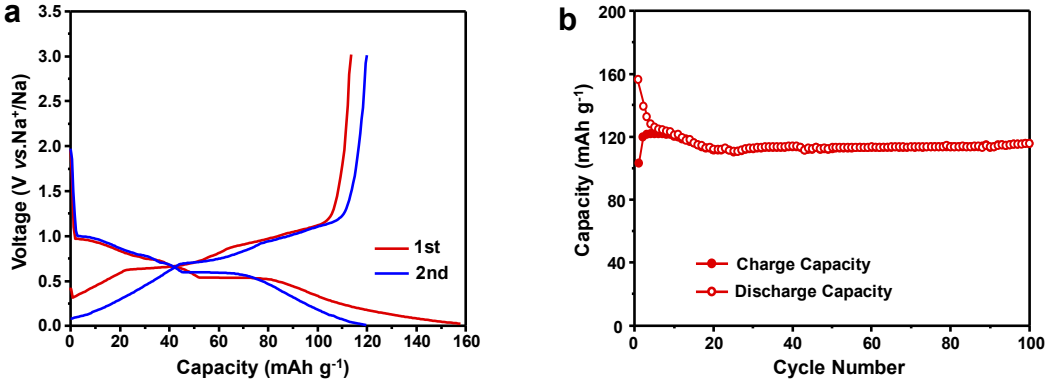

Fig. S6 (a) Galvanostatic discharge/charge profiles and (b) cycle performance of the pure graphite anode at 100 mA g^{-1} for SIBs.

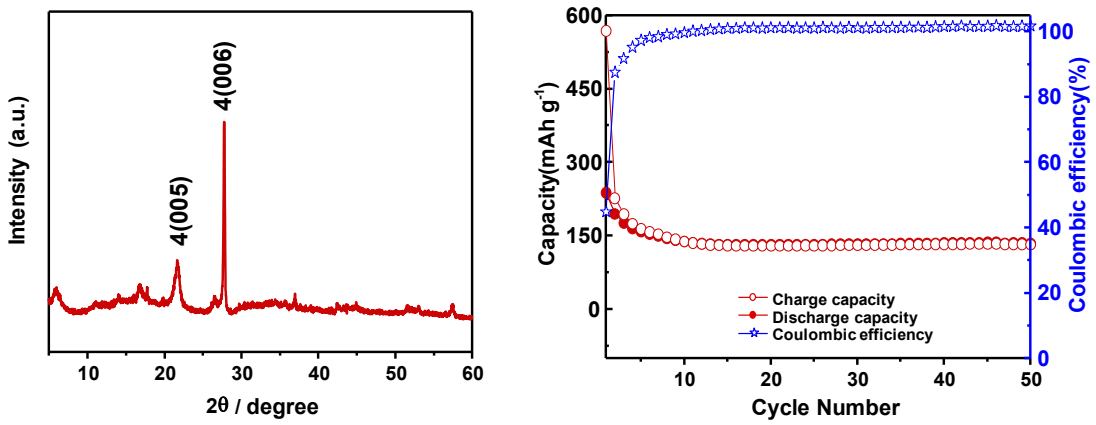

Fig. S7 XRD pattern of the $MoCl_5$-GIC-4 and cycle performance at 100 mA g^{-1} for SIBs.

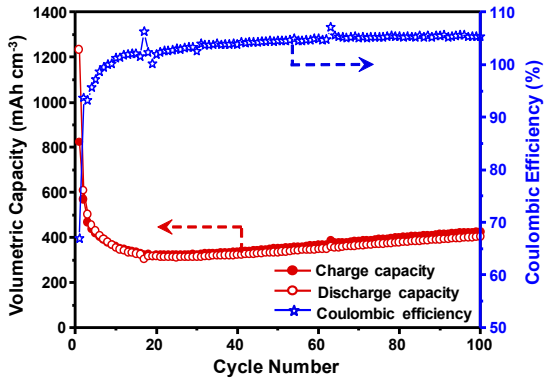

Fig. S8 Cycle performance of $MoCl_5$-GIC-1 with the volumetric capacities and coulombic efficiencies for SIBs.

Table S1. Comparison of electrochemical data of $MoCl_5$-GIC in this work with previously reported $FeCl_3$-intercalated GIC anode materials for lithium-ion batteries.

Sample	Type of battery	Capacity (mAh g^{-1}) at different current densities (A g^{-1})			Cycle Number	Ref.
$MoCl_5$-GIC	**LIB SIB**	**0.2/1099 0.1/275**	**1/600 1/155**	**2/512 5/72**	**150 1000**	**This work**
$FeCl_3$-GIC	LIB	0.1/500	1/350	5/260	400	[1]
$FeCl_3$-MGIC	LIB	0.2/847	0.4/677	1.5/218	100	[2]
$FeCl_3$-FLG	LIB	0.2/810	1/500	2/415	50	[3]
C–Cl/$FeCl_2$/C–Cl	LIB	0.2/615	1/408	3/298	1000	[4]
$FeCl_3$-HOGIC	LIB	0.2/1371	1/963	5/192	50	[5]
Fe_2O_3/ $FeCl_3$-GIC	LIB	0.2/845	1/563	2/260	300	[6]
$NiCl_2$-GICs	LIB	0.1/442	—	—	50	[1]
$CoCl_2$-GICs	LIB	0.1/423	—	—	50	[1]

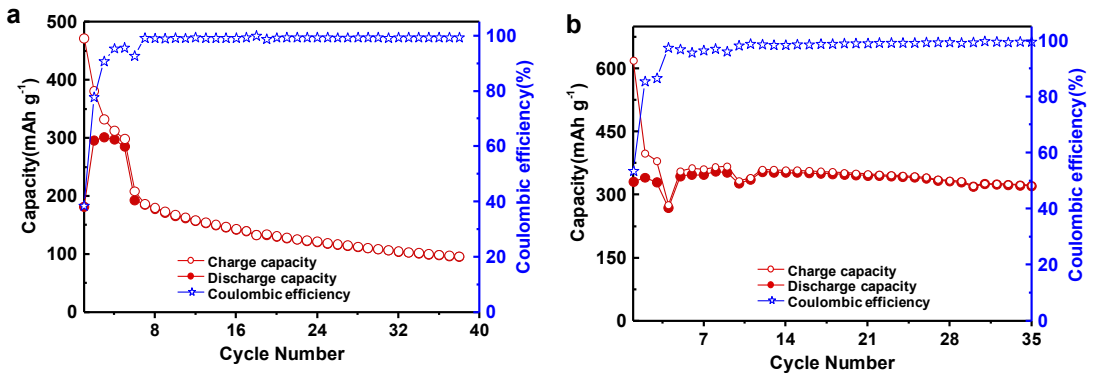

Fig. S9 Cycle performance of the physically mixed $MoCl_5$ and graphite: (a) sodium storage at 100 mA g^{-1}; (b) lithium storage at 200 mA g^{-1}.

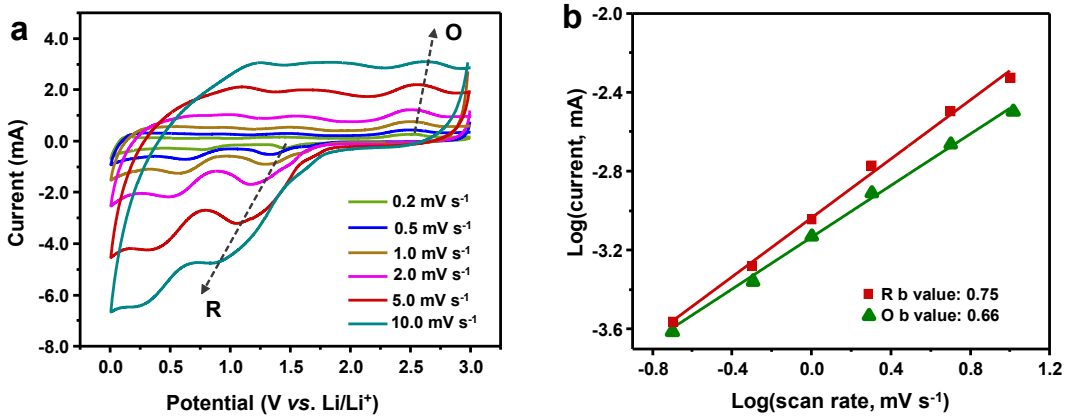

Fig. S10 (a) CV curves at different scan rates, and (d) relationship between logarithm current *vs*. logarithm scan rate of $MoCl_5$-GIC-1 for LIBs.

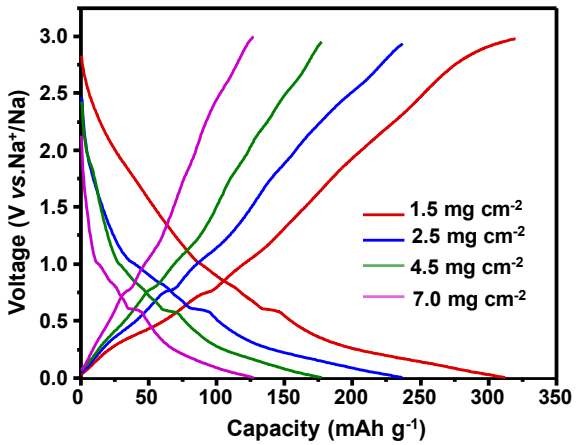

Fig. S11 Galvanostatic discharge/charge voltage profiles of $MoCl_5$-GIC-1 with different mass loadings for SIBs.

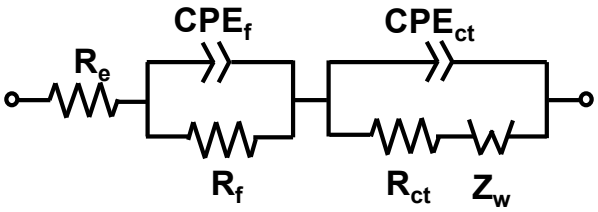

Fig. S12 Equivalent electrical circuit for fitting electrochemical impedance data.

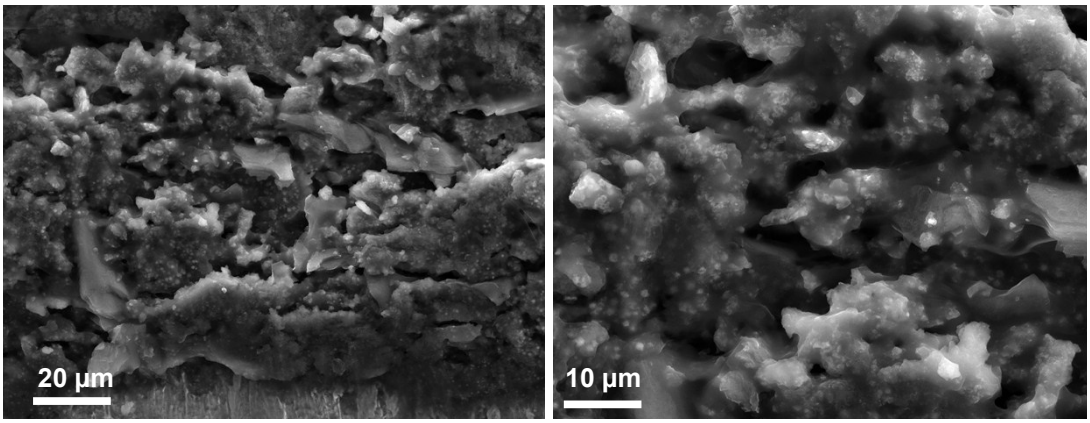

Fig. S13 SEM images of the $MoCl_5$-GIC-1 anodes after 100 fully sodiation/desodiation cycles.

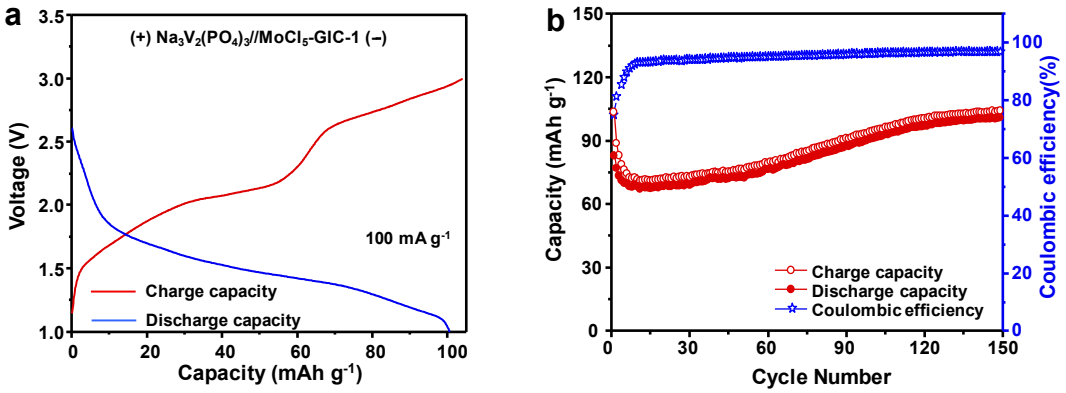

Fig. S14 (a) Representative galvanostatic charge/discharge profile and (b) cycle performance of a full cell assembled with a $Na_3V_2(PO_4)_3$ cathode and $MoCl_5$-GIC-1 anode at 100 mA g^{-1}.

References

1. F. Wang, J. Yi, Y. Wang, C. Wang, J. Wang and Y. Xia, *Adv. Energy Mater.*, 2014, **4**, 1300600.

2. X. Qi, J. Qu, H.-B. Zhang, D. Yang, Y. Yu, C. Chi and Z.-Z. Yu, *J. Mater. Chem.*

A, 2015, **3**, 15498-15504.

3. L. Wang, C. Guo, Y. Zhu, J. Zhou, L. Fan and Y. Qian, *Nanoscale*, 2014, **6**, 14174-14179.

4. Y. Sn, F. Han, C. Zhang, F. Zhang, D. Zhou, H. Liu, C. Fan, X. Li and J. Liu *Energy Tech.*, 2019, **7**, 1801091.

5. C. Zhang, F. Han, J. Ma, Z. Li, F. Zhang, S. Xu, H. Liu, X. Li, J. Liu and A.-H. Lu, *J. Mater. Chem. A*, 2019, **7**, 11771-11781.

6. Z. Li, C. Zhang, F. Han, F. Zhang, D. Zhou, S. Xu, H. Liu, X. Li and J. Liu, *Nano Res.*, 2019, **12**, 1836-1844.